Monitoring Botulinum Neurotoxin A Activity with Peptide-Functionalized Quantum Dot Resonance Energy Transfer Sensors

Kim E. Sapsford,[†,*] Jessica Granek,[†] Jeffrey R. Deschamps,[‡] Kelly Boeneman,[‡] Juan Bautista Blanco-Canosa,[⊥] Philip E. Dawson,[⊥] Kimihiro Susumu,[§] Michael H. Stewart,[§] and Igor L. Medintz[‡,*]

[†]Division of Biology, Office of Science and Engineering Laboratories, U.S. Food and Drug Administration, Silver Spring, Maryland 20993, United States, [‡]Center for Bio/Molecular Science and Engineering Code 6900, and [§]Optical Sciences Division Code 5600, U.S. Naval Research Laboratory 4555 Overlook Avenue, S.W., Washington, D.C. 20375, United States, and [⊥]Departments of Cell Biology and Chemistry, The Scripps Research Institute, La Jolla, California 92037, United States

ABSTRACT Botulinum neurotoxins (BoNTs) are extremely potent bacterial toxins that contaminate food supplies along with having a high potential for exploitation as bioterrorism agents. There is a continuing need to rapidly and sensitively detect exposure to these toxins and to verify their active state, as the latter directly affects diagnosis and helps provide effective treatments. We investigate the use of semiconductor quantum dot (QD)—peptide Förster resonance energy transfer (FRET) assemblies to monitor the activity of the BoNT serotype A light chain protease (LcA). A modular LcA peptide substrate was designed and optimized to contain a central LcA recognition/cleavage region, a unique residue to allow labeling with a Cy3 acceptor dye, an extended linker-spacer sequence, and a terminal oligohistidine that allows for final ratiometric peptide—QD-self-assembly. A number of different QD materials displaying charged or PEGylated surface-coatings were evaluated for their ability to self-assemble dye-labeled LcA peptide substrates by monitoring FRET interactions. Proteolytic assays were performed utilizing either a direct peptide-on-QD format or alternatively an indirect pre-exposure of peptide to LcA prior to QD assembly. Variable activities were obtained depending on QD materials and formats used with the most sensitive pre-exposure assay result demonstrating a 350 pM LcA limit of detection. Modeling the various QD—peptide sensor constructs provided insight into how the resulting assembly architecture influenced LcA recognition interactions and subsequent activity. These results also highlight the unique roles that both peptide design and QD features, especially surface-capping agents, contribute to overall sensor activity.

KEYWORDS: Förster resonance energy transfer · FRET · quantum dot · peptide · protease · metal affinity · botulinum neurotoxin A · biosensor · fluorescence · biothreat agent · nanocrystal · semiconductor

Clostridial botulinum neurotoxins, serotypes A through G (BoNT A—G), are considered the most potent protein toxins known to humans and cause neuroparalytic disease.[1,2] BoNTs are synthesized as single chain precursors and become activated through post-translational proteolysis forming a dimeric structure comprising both light (Lc ≈ 50 kDa) and heavy (Hc ≈ 100 kDa) chains linked *via* a disulfide bond.[1,2] Following *in vivo* exposure, BoNTs are endocytosed into presynaptic nerve cells where the disulfide bond is reduced releasing BoNT Lc into the cytosol as an active zinc-dependent endopeptidase. This protein targets specific SNARE (soluble *N*-ethylmaleimide-sensitive factor attachment protein receptor) proteins leading to inhibition of acetylcholine release and producing neuroparalysis.[1−3] SNARE protein targets for each of the BoNT-Lcs are serotype dependent, with the BoNT A examined here (referred to as LcA hereon), cleaving a specific region of synaptosomal-associated protein 25 (SNAP-25).[1,4] Although they do have some clinical and cosmetic utility, BoNTs are still considered to be naturally occurring food pathogens and a significant biothreat due to their potential for use in bioterrorism.[3,5] Technologies providing rapid, sensitive, and specific detection of BoNT exposure remain essential for providing timely diagnosis and effective treatments.[3,5,6]

The "gold-standard" mouse-lethality test is currently the only widely accepted method of confirming BoNT exposure. The majority of the remaining BoNT detection approaches involve either immunological-based assays, endopeptidase activity assays, or some combination of the two (reviewed in refs 2 and 3). LcA is the most commonly studied target, and various immunoassay formats have been demonstrated for it including those utilizing fluorescence, enzyme linked immunosorbent assay (ELISA), surface plasmon resonance (SPR), or electrochemiluminescence.[2,3,7] While immunoassays have demonstrated low picogram limits of detection (LOD), most formats require significant sample preparation and incorporate multiple reagent and assay steps prior to

* Address correspondence to Kim.Sapsford@fda.hhs.gov; Igor.Medintz@nrl.navy.mil.

Received for review November 5, 2010 and accepted February 10, 2011.

Published online February 28, 2011
10.1021/nn102997b

detection. Immunoassays also do not provide information regarding the active state of the enzyme. Assays to determine LcA activity typically incorporate peptide-based substrates and fall into three functional groups based on the format exploited: (1) monitoring mass changes due to substrate cleavage *via* mass spectroscopy, cantilever, ultraperformance liquid chromatography, or SPR analysis; (2) monitoring changes in Förster resonance energy transfer (FRET) upon peptide cleavage; (3) antibodies targeting a cleaved portion of the substrate.[2,3,8−10] Combined strategies where agarose beads functionalized with antibodies were used to capture LcA followed by the introduction of a fluorogenic peptide substrate have yielded attogram limits of detection (LODs).[11] The principle advantages of FRET-based assays are that the signal is transduced directly upon addition of the target and proteolysis (*i.e.,* one-step) while simultaneously confirming enzyme activity. Simplified FRET-based assays are also far more amenable to integration into lab-on-a-chip (LOC) devices for field deployment.[12−14] However, the photophysical properties of the organic dyes commonly utilized in most FRET-based assays continue to be problematic. These fluorophores can suffer from pH-sensitivity, low quantum yields, photobleaching, and chemical degradation which, along with their broad-overlapping absorption spectra, significantly complicate FRET formats and subsequent data analysis.[15]

The growing utility of semiconductor nanocrystals or quantum dots (QDs) can help address many of these issues. As FRET donors and acceptors, QDs are physiochemically robust and manifest unique photophysical properties which are cumulatively unavailable to conventional organic dyes in the same role.[16−20] These include the ability to utilize specific QD emissions to optimize spectral overlap with a given acceptor, array multiple acceptors around a central QD scaffold which controllably increases energy transfer, excite the QD donor at a wavelength that corresponds to an acceptor absorbance minimum thus reducing direct acceptor excitation, and access to multiplex FRET configurations.[16−18] We, and several other groups, have utilized QDs conjugated to designer peptide or protein substrates to monitor the activity of many proteases including trypsin, caspase 1, caspase 3, thrombin, chymotrypsin, along with collagenase and several matrix metalloproteinases.[21−25] Interestingly, most of these proteases require rather limited sequences for substrate cleavage. Trypsin, for example, proteolyzes peptide chains on the carboxyl side of lysine or arginine residues.[23] The BoNT Lc's, in contrast, are among the most selective proteases known.[1] LcA recognizes an optimum substrate sequence comprising 16 residues found in the SNAP25 protein.[26] The use of such long, specific sequences in compact QD−peptide sensors has not yet been verified.

Here, we describe the use of QD−peptide assemblies for monitoring specific BoNT LcA activity. The design and sequence of a modular peptide was iteratively improved for assembly onto QDs and use as the LcA substrate. Four different QD materials, including two custom-synthesized and two commercially available QD preparations, with either charged or PEGylated surface-coatings were initially tested via FRET for their ability to self-assemble the dye-labeled LcA peptide substrate. Proteolytic assays were then performed utilizing either a direct "On-QD" format or alternatively an indirect "Off-QD" format consisting of pre-exposure of peptide to LcA followed by subsequent QD assembly, see Figure 1. Various activities were obtained which depended upon QD materials and assay formats used. Modeling studies were also undertaken to better understand the roles that peptide design and QD characteristics, including surface-capping ligand, impart to sensor activity.

RESULTS AND DISCUSSION

A detailed description of the materials and procedures used, including all data analysis, can be found in the Materials and Methods section.

Peptide Structure and Self-Assembly to Quantum Dots. Pretesting of assay formats utilized a Cy3-acceptor labeled version of the initial peptide sequence shown in Figure 1B. This was based on a consensus of commercial substrate sequences.[27] Self-assembly to both DHLA and DHLA-PEG QDs verified efficient FRET between the QD donors and the Cy3 (data not shown). However, exposure of LcA to this peptide sequence, both when QD assembled (On-QD) and when in solution alone (Off-QD), did not result in any proteolysis even after extended incubation times. We thus modified the peptide substrate design and sequence in an effort to facilitate proteolysis, see Figure 1B. The core LcA recognized binding/substrate site was extended from a minimal 13 residues to 16, which includes the full SNAP-25 sequence from residues 187−202, and the central glutamic acid (E) 194 was modified to a glutamine (Q).[26] This substitution was based upon the extensive kinetic studies by Schmidt and Bostian, who investigated various amino acid replacements within designer LcA peptide substrates and their effect on proteolytic activity.[26] The E→Q substitution chosen demonstrated a 2-fold increase in the relative rate of LcA cleavage. The N-terminal cysteine was also moved away from the LcA site by inclusion of an extra serine residue in an effort to prevent dye-attachment from interfering with protease binding. The initial peptide had incorporated a $(Pro)_7$ sequence as the helical spacer. This is assumed to form a type II helix with a predicted linear extension of ~14 Å.[28] Some evidence, however, suggests that these types of polyproline structures may undergo frequent cis-to-trans isomerization which could create a structure that bends back

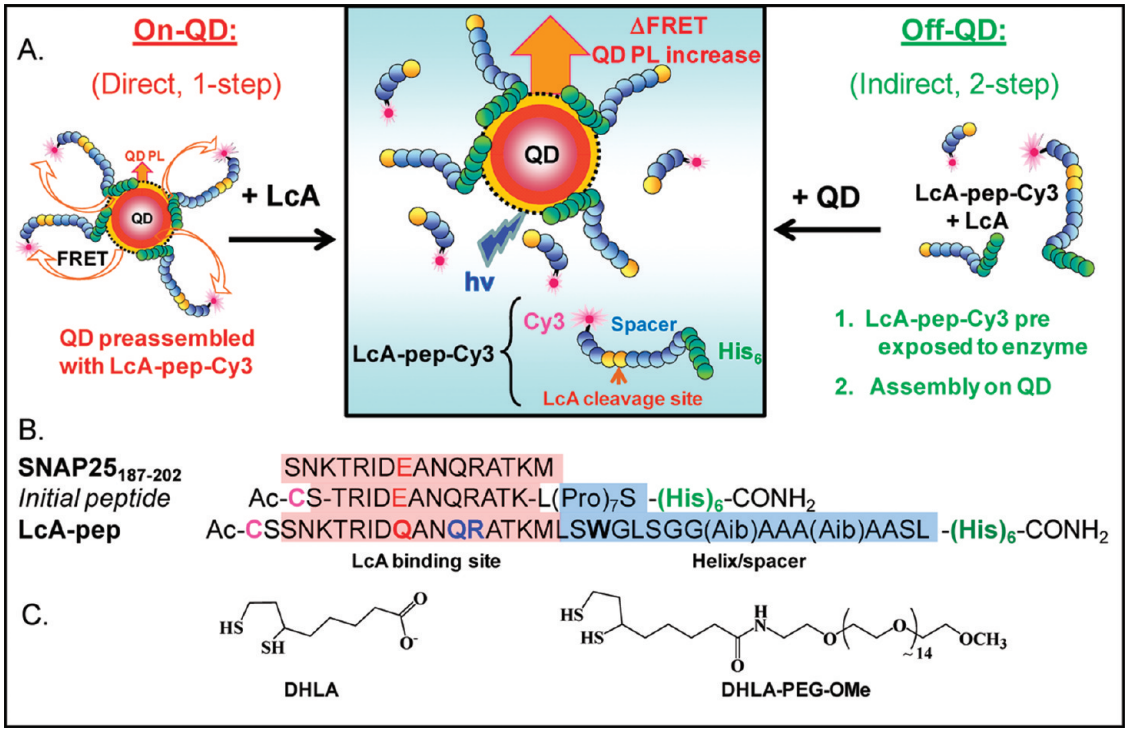

Figure 1. QD-FRET assay design components. (A) Schematic illustrating the two QD-FRET-based assay formats, On-QD (one-step) and Off-QD (two-step), used to investigate LcA enzymatic activity. (B) Peptide sequences of the LcA substrate used in this study. Aib is alpha-amino isobutyric acid, Ac is a *N*-terminal acetyl blocking group, and $CONH_2$ is a C-terminal amide blocking group. Colors are used to highlight the different functional modules. (C) Chemical structures of the two capping agents, DHLA and DHLA-PEG, used to render the in-house synthesized QDs hydrophilic.

upon itself.[28] Given that the central portion of the LcA substrate sequence already has a critical bend in its structure, the insertion of a second bend into the sequence could be detrimental, inducing the peptide to wrap completely back upon itself and make the substrate portion completely inaccessible to the LcA, see modeling below. We thus replaced the $(Pro)_7$ sequence with the 7-alanine/artificial alpha-amino isobutyric acid (Aib) residue sequence. Aib when used in combination with alanines induces rigid-helical structures. Although considered part of the spacer, glycines were inserted after the helix to "break" this structural motif.[21] Several serine and leucine residues were also inserted for length and flexibility. Overall, it was anticipated that the longer helix/spacer spacer would more than double the distance between the QD surface and the LcA binding site, and indeed this extended length would prove crucial to the peptide's ability to function as a substrate while assembled on the QD (*vide infra*).

The final LcA peptide substrate sequence (LcA-pep) used is shown in Figure 1B. Similar to the other proteolytic peptidyl substrates we have used with QDs,[21,23,29,30] it can best be described as consisting of several functional modules arranged in a sequential order. The C-terminus displays the $(His)_6$ metal-affinity sequence, shown in green, which facilitates QD attachment *via* two closely related interactions. We, along with several other groups, have shown that oligohistidine sequences drive self-assembly of proteins, peptides, and appropriately modified DNA to QDs made soluble with bifunctional thiolated ligands.[31−37] This high-affinity binding interaction (equilibrium binding constant of $K_d \approx 1$ nM) occurs between the imidazolium side chain groups on the oligohistidine-sequences and the Zn^{2+}-rich surface of CdSe/ZnS core/shell QDs.[31] For ITK QDs made soluble with amphiphilic block-copolymer-type surface ligands that prevent access to the Zn shell, a similar type of binding is sometimes possible.[38] In this case, it is surmised that carboxylated derivatives of these ligands coordinate divalent cations in a manner analogous to that found on nitrilotriacetic acid-chelate media which is commonly used for protein and peptide purification.[32,36,39,40] Indeed, Rao's group has shown that adding Ni^{2+} to QDs functionalized with these ligands can significantly increase the amount of coordinated $(His)_6$-protein.[25] Despite the subtle differences between these two related interactions, self-assembly in each case will follow a Poisson-type process and control over the ratio of peptide/QD can be exerted through the molar ratios of each used.[36,41,42] Immediately adjacent to the $(His)_6$ sequence is the helix/spacer module shown in blue which is used to extend the rest of the peptide sequence away from the QD surface. A tryptophan was inserted into the peptide to provide UV absorption for monitoring the native peptide. The next module shown in pink contains the LcA substrate recognition portion where the E→Q substitution is highlighted in

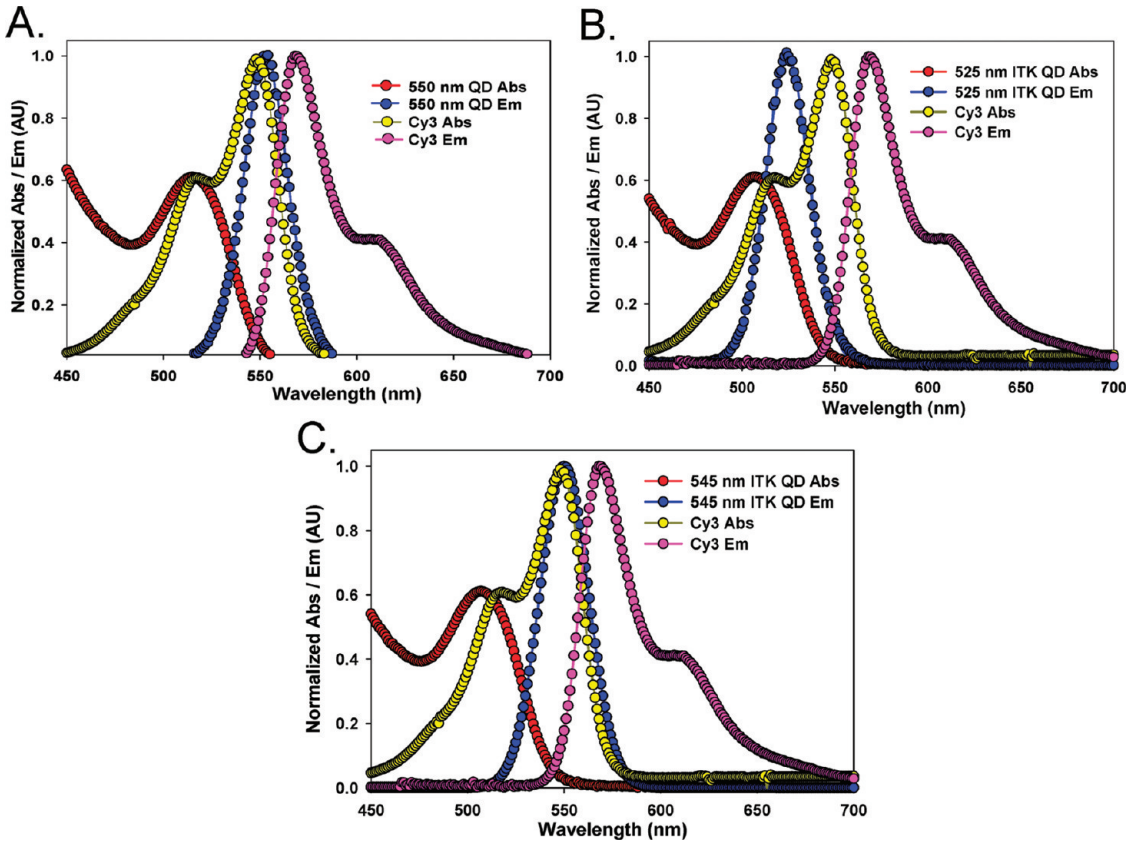

Figure 2. Spectral overlap profiles for FRET donor and acceptor species used in this study. (A) Normalized absorption and emission profiles of the 550 nm QD DHLA (donor) and Cy3 (acceptor). The same QDs were also functionalized with DHLA-PEG. (B) Normalized absorption and emission profiles of the commercial 525 nm ITK QD (donor) and Cy3 (acceptor). (C) Normalized absorption and emission profiles of the commercial 545 nm ITK QD (donor) and Cy3 (acceptor).

red. The QR residues in blue show the site of LcA cleavage within this sequence. Lastly, the peptides N-terminal cysteine provides a unique thiol handle for site-specific dye-modification of the peptide.

Quantum Dots and Spectral Overlap. We utilized four different QD samples which can be grouped into two categories based upon the surface functionalization chemistry used to make them water-soluble. The first type consists of QDs made hydrophilic with either DHLA or PEG-appended DHLA, see Figure 1C. Although structurally related, these DHLA-based ligands provide a different set of benefits and liabilities for nanocrystal solubilization. Both utilize the dithiol motif for strong binding interactions with the QD surface. With a MW of ~206 and a predicted lateral extension of 10−12 Å,[43,44] DHLA is among the smallest ligands available for solubilizing nanoparticles.[45,46] DHLA provides colloidal stability to the QDs *via* the charge on its terminal carboxyl group; however, this also limits dispersions to the basic pH regime. In contrast, poly(ethylene glycol) mediates the solubility of the DHLA-PEG coated QDs in a relatively pH independent manner.[47−49] However, the number of these repeats (~14 to 15) results in a significant increase in the overall mass and size of this ligand relative to DHLA (MW ≈ 926, predicted extension of 30−38 Å as attached to QD).[44] Regardless of these structural differences, it has been repeatedly demonstrated that His_6-appended peptides and DNA can penetrate the coatings of QDs prepared with either of these ligands and rapidly attach to the QD ZnS surface.[23,30] However, the bulk size of His_6-appended proteins combined with PEG steric effects generally prevent self-assembly of these larger, globular structures to the latter type of QD preparation.[31] Recent studies suggest that DHLA-functionalized QDs can display on average 50 ± 10 $(His)_6$-peptides on their surfaces.[43] The second type of QD are assumed to be surface-functionalized with a proprietary carboxylated amphiphilic poly(acrylic acid) -based block copolymer.[36,38,40] The large size of this coating layer significantly increases the hydrodynamic radius of these QD preparations to values approaching >7.5 nm in size according to manufacturers specifications (www.lifetechnologies.com).[40] As mentioned above, the His_6-metal affinity sequence is not expected to penetrate the polymer but rather to coordinate to the surface carboxyl groups especially in the presence of divalent cations. When appropriately arranged, carboxyl groups are known for their high affinity chelation of divalent cations.[39]

Within these proteolytic sensors, changes in FRET *E* form the basis of signal transduction and thus spectral

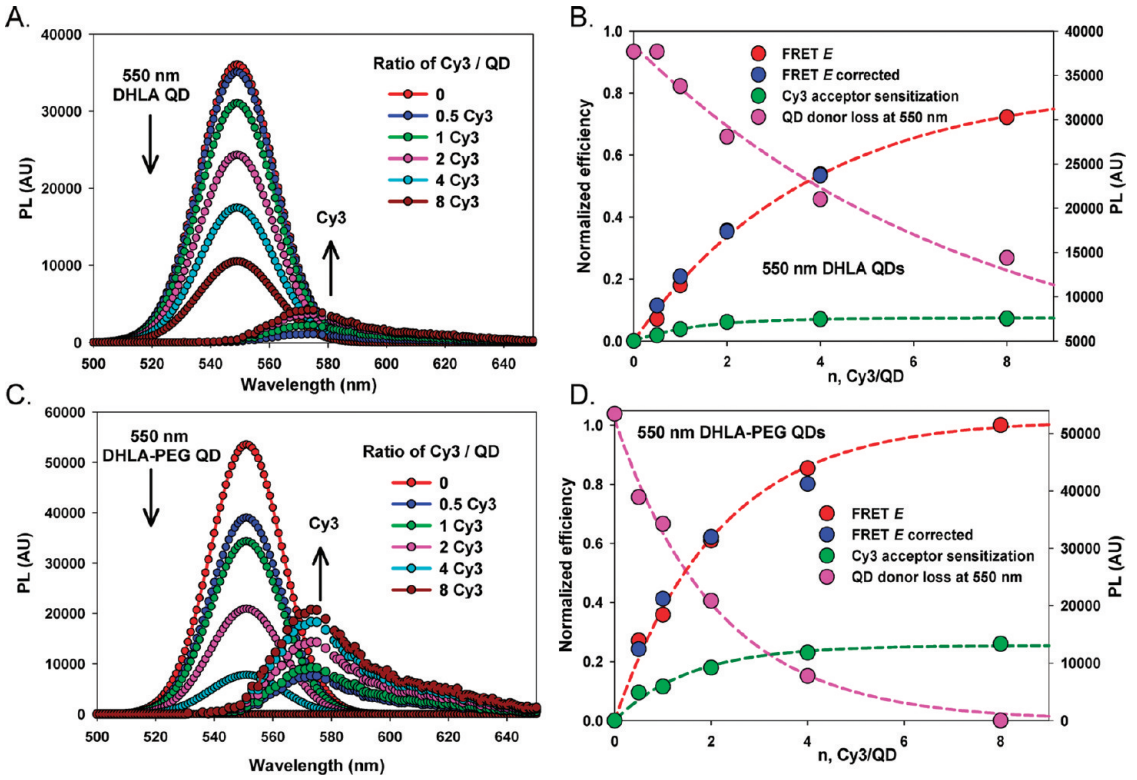

Figure 3. QD-to-Cy3-peptide FRET efficiency for DHLA, DHLA-PEG QDs. (A) PL spectra resulting from assembling an increasing number of Cy3-LcA-pep per 550 nm DHLA-QDs. (B) The QD donor PL intensity loss at 550 nm (pink, units of PL right axis) is plotted as a function of the number of Cy3-LcA-pep/QD, along with the sensitized Cy3 acceptor emission (green) at 570 nm. The corresponding FRET *E* (red) and the corrected FRET *E* (blue) determined from panel A, using the integrated area under the curve, are plotted as a function of the number of Cy3-LcA-pep/QD. (C) PL spectra resulting from assembling an increasing number of Cy3-LcA-pep per 550 nm DHLA-PEG-QDs. (D) The QD donor PL intensity loss at 550 nm (pink, units of PL right axis) is plotted as a function of the number of Cy3-LcA-pep/QD, along with the Cy3 acceptor emission (green) at 570 nm. The corresponding FRET *E* (red) and the corrected FRET *E* (blue) determined from (C), using the integrated area under the curve, are plotted as a function of the number of Cy3-LcA-pep/QD. Lines of best fit are added to the efficiency plots to guide the eye.

overlap is a critical parameter for optimized function. Ideally, the donor−acceptor pairing in each QD-sensor should manifest both efficient FRET and demonstrate significant changes in *E* following proteolysis.[2] To focus more closely on QD effects, the LcA-pep was labeled solely with Cy3 which is utilized as a "universal" FRET acceptor in these assays. Given the differences in DHLA ligand structures, we opted to use the same 550 nm emitting core−shell QDs for both DHLA-based samples. Figure 2A shows the normalized absorption and emission of the 550 nm QD donor superimposed over that of the Cy3 acceptor. A nominal QY of 20% was determined for both QD samples by comparison to a dye standard (Rhodamine 6G in methanol $\Phi_f = 0.93$) and yields a predicted Förster distance (R_0) value of 56 Å for this donor−acceptor pair. Since the ITK QDs have the same surface chemistry, we opted here to vary spectral overlap by using 2-different QD emissions. The 525 nm QDs as supplied have a reported QY of 84%, yielding a predicted R_0 value of 48 Å with the Cy3 acceptor. Improving overlap by switching to a QD sample with an emission maxima centered at 545 nm and a reported QY of 78%, significantly increases the R_0 value with Cy3 by ~two-thirds to 73 Å (see Figure 2B,C). The high QY of these QDs results in part from their polymer overcoating which encapsulates the nanocrystals preventing water from gaining access to the surface and increasing QD passivation.[40]

Characterizing FRET Efficiency. We began by monitoring changes in QD−peptide FRET *E* as increasing ratios of LcA-pep-Cy3 were self-assembled onto the various QD preparations to verify formation of the complexes and to understand the underlying photophysical processes. Figure 3A presents deconvoluted, direct-acceptor excitation corrected PL spectra for 550 nm DHLA QDs self-assembled with the indicated ratios of Cy3-acceptor labeled peptide. All QD emissions are shown fitted to a Gaussian profile. Data collected from equivalent amounts of Cy3 acceptor alone illuminated at the same wavelength were used for correcting the direct acceptor excitation component. Panel 3B plots the corresponding loss of QD donor PL, normalized FRET *E*, FRET *E* corrected for heterogeneity, and the Cy3 acceptor sensitization as a function of acceptor valence. Analysis of this data using eqs 2 and 3 (described in detail in the Materials and Methods section) derives a QD-donor to Cy3-acceptor center-to-center separation distance *r* of 69 Å. Figure 3C shows spectra collected in the same

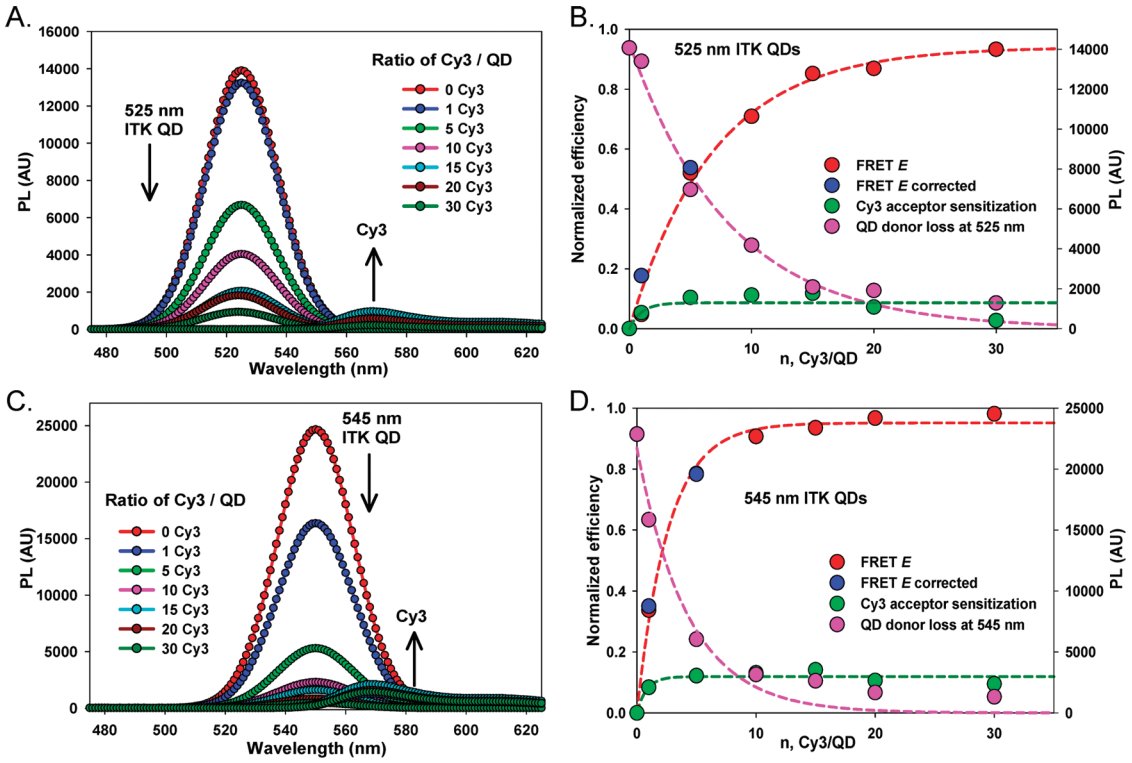

Figure 4. QD-to-Cy3-peptide FRET efficiency for ITK QDs. (A) PL spectra resulting from assembling an increasing number of Cy3-LcA-pep per 525 nm ITK QDs. (B) The QD donor PL intensity loss at 525 nm (pink, units of PL right axis) is plotted as a function of the number of Cy3-LcA-pep/QD, along with the Cy3 acceptor emission (green) at 570 nm. The corresponding FRET *E* (red) and the corrected FRET *E* (blue) determined from panel A, using the integrated area under the curve, are plotted as a function of the number of Cy3-LcA-pep/QD. (C) PL spectra resulting from assembling an increasing number of Cy3-LcA-pep per 545 nm ITK QDs. (D) The QD donor PL intensity loss at 545 nm (pink, units of PL right axis) is plotted as a function of the number of Cy3-LcA-pep/QD, along with the Cy3 acceptor emission (green) at 570 nm. The corresponding FRET *E* (red) and corrected FRET *E* (blue) determined from panel C, using the integrated area under the curve, are plotted as a function of the number of Cy3-LcA-pep/QD. Lines of best fit are added to the both efficiency plots.

manner from 550 nm DHLA-PEG QD donors self-assembled with the same ratios of labeled peptide while panel 3D plots the corresponding values *versus* acceptor valence. A center-to-center separation distance *r* of 56 Å is derived from analyzing this data. Similar trends are noted for both QD samples including relatively efficient FRET *E* approaching 80 and 100% at ratios of 8 acceptors along with modest acceptor sensitization corresponding to a maximum of 10, and 20% for the DHLA and DHLA-PEG QDs, respectively.

Surprisingly, a larger separation distance and lower FRET *E* is observed with the smaller DHLA ligands while a closer separation distance is observed with the larger PEGylated ligands. These results are counterintuitive as the PEG layer is anticipated to sterically prevent a close approach of the acceptor-dye. We attribute this unexpected result to the complex interplay between the different types of QD surface ligands and the lateral dye-labeled portion of the peptide. At the pH of 8 used, the terminal LcA binding portion of the peptide is anticipated to have a charge of $\sim^{+}2.5$ (http://www.scripps.edu/~cdputnam/protcalc.html) and this may act in a repulsive manner to keep the dye further away from the QD. We hypothesize that the PEG ligands constrain the helix-linker portion of the peptide to extend laterally away from the QD surface and also minimize charge-based repulsion. However, the bend in the peptide probably forces the Cy3 at the opposite end of the structure to physically interdigitate or penetrate with the ends of the surrounding PEG layer (*vide infra*). The PEG layer will display a far less dense arrangement at its termini than when moving closer into the spherical QD surface which may also contribute to this result.

Figure 4 shows FRET data collected from the carboxylated ITK QDs in a similar manner to that shown above. Figure 4 panels A and C show the deconvoluted and direct-acceptor excitation corrected PL spectra for the 525 and 545 nm emitting QDs, respectively, while panels B and D show the corresponding loss of QD donor PL, normalized FRET *E*, FRET *E* corrected, and the Cy3 acceptor sensitization as a function of acceptor valence. Again similar trends are observed for both QD samples when assembled with this dye acceptor peptide. The 525 nm QDs are more than 80% quenched by a ratio of 15 peptides/QD, whereas the 545 nm QDs reach this quenching level at around only 5 peptides/QD clearly reflecting the significantly better spectral overlap. Cy3 acceptor sensitization is quite low in both samples regardless of ratio or spectral overlap and appears to plateau at approximately 10% in both cases.

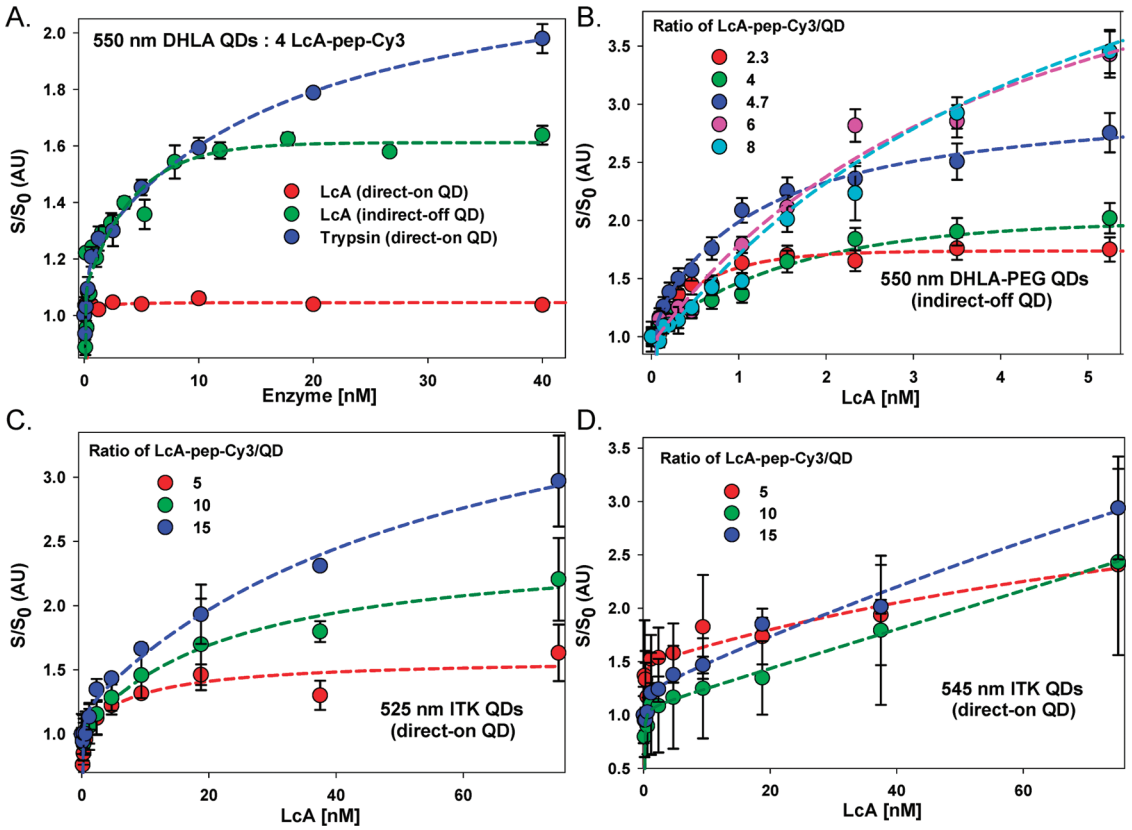

Figure 5. LcA protease activity assays. (A) LcA protease activity assays using 550 nm DHLA QDs modified with 4 LcA-pep-Cy3; the increase in QD PL is plotted as S/S_0 (relative to LcA-pep-Cy3-QD construct not exposed to enzyme) *versus* enzyme concentration using either the On-QD (red) or Off-QD (green) incubation for LcA [data replicates $n = 2-4$; LOD Off-QD, 0.308 nM] and an On-QD incubation for trypsin (blue) [$n = 3$; LOD, 0.625 nM]. (B) LcA protease activity assays using 550 nm DHLA-PEG QDs modified with different ratios of LcA-pep-Cy3, the increase in QD PL is plotted as S/S_0 (relative to LcA-pep-Cy3-QD construct not exposed to enzyme) as a function of LcA concentration using a Off-QD incubation [$n = 6$; LODs, acceptor ratio of 2.3 = 0.1 nM; 4 = 0.5 nM; 4.7 = 0.1 nM; 6 = 0.3 nM; 8 = 0.7 nM]. (C) LcA protease activity assays using commercial 525 nm ITK QDs modified with different ratios of LcA-pep-Cy3, the increase in QD PL is plotted as S/S_0 (relative to LcA-pep-Cy3-QD construct not exposed to enzyme) as a function of LcA concentration using an On-QD incubation [$n = 2-4$; LODs, acceptor ratio of 5 = 2.3 nM; 10 = 18.8 nM; 15 = 2.3 nM], data after 3 h incubation. (D) LcA protease activity assays using commercial 545 nm ITK QDs modified with different ratios of LcA-pep-Cy3, the increase in QD PL is plotted as S/S_0 (relative to LcA-pep-Cy3-QD construct not exposed to enzyme) as a function of LcA concentration using an On-QD incubation [$n = 2-4$; LODs, acceptor ratio of 5 = 4.7 nM; 10 = 37.5 nM; 15 = 1.2 nM]. Data after 3 h incubation.

Interestingly, this low level of acceptor sensitization is not uncommon when performing FRET studies with similar commercially obtained QD materials and has been frequently observed with 605 nm QDs when paired with structurally similar Cy5 acceptor dyes in different formats; it is believed to arise from the low acceptor quantum yield when sensitized by a donor.[50,51] Analyzing the FRET data with eqs 2 and 3 derives a QD-donor to Cy3-acceptor center-to-center separation distance r of 59 and 74 Å for complexes assembled with the 525 and 545 nm QDs, respectively. The larger separation distance for the 545 nm QDs can be partially ascribed to their slightly larger radius. The ITK QD−peptide complexes were assembled in buffer supplemented with excess Ni^{2+}. Similar to Rao's finding,[25] assembling the same complexes in the absence of Ni^{2+} resulted in far lower FRET E (data not shown). Mixing QD control solutions with equivalent amounts of free Cy3-acceptor dye resulted in a modest quenching that could be fit to a Stern−Volmer function indicative of solution-phase interactions (data not shown). This confirms that $(His)_6$-driven metal affinity assembles the peptides on to the QD surface. Agarose gel electrophoresis of select QD-conjugates also confirmed peptide self-assembly (data not shown). Equation 3 was only applied at ratios of $n \leq 5$, to probe for any deviance arising from heterogeneity during self-assembly, and this is shown as the blue points in Figures 3 and 4 panels B and D. The strong correspondence between normalized FRET E and FRET E corrected indicates that this is not an issue in these assemblies and would not alter the outcome.

Proteolytic Assays. We began testing the final LcA-pep-Cy3 in combination with 550 nm DHLA-functionalized QDs. A ratio of four peptides-per-QD was utilized based upon the criteria of efficient FRET and the possibility of significant changes in FRET E following proteolysis as iterated above. This valence corresponds to a FRET E of ~50% and reduction of this ratio by proteolysis accesses the more dynamic portion of

the curve shown in Figure 3B. Exposing the preassembled QD−peptide sensors to increasing LcA concentrations for 3 h incubations did not, however, result in any visible FRET changes indicating the absence of proteolysis (see Figure 5A, LcA direct-on QD data). Similar results were also obtained with DHLA-PEG QDs (data not shown). This was followed by 2 subsequent experiments which would serve to be diagnostic of the underlying issues. In the first, the same DHLA-QD−peptide assemblies were exposed to increasing concentrations of trypsin for 2 h at room temperature. This protease should cleave this peptide substrate at four different sites (C-terminal to the K or R residues) which are all located in the LcA binding site portion. The resulting data shown in Figure 5A, where changes in QD donor PL are converted to S/S_0 ratios (as explained in the Materials and Methods section), indicated that the peptide was quite effectively cleaved by trypsin when attached to the QD. This is analogous to previous results where QDs decorated with a peptide of similar sequence were also exposed to trypsin.[28] Interestingly, the LOD (concentration where signal is greater than the blank plus three times its standard deviation) for trypsin was 0.625 nM enzyme which is a factor of 10 lower than the 6.2 nM determined in that previous study. In the second experiment, the equivalent of ~4 LcA-pep-Cy3 were preincubated with LcA using the indirect Off-QD format for 2 h and then mixed with the QDs for 30 min prior to fluorescent data collection. The dose response increase collected from this data clearly indicate that the LcA is quite active with solution-phase peptide and allowed a LOD of 0.308 nM enzyme to be derived. Combined, these two experiments strongly suggest that the far larger LcA, as compared to trypsin (MW ≈ 50 *vs* 24 kD), is sterically precluded from productive interactions with the peptide substrate once assembled on the QD. However, performing the assay in two parts (indirect and Off-QD) could still allow viable assay data to be collected with the same substrate materials.

On the basis of the above results, we next applied the indirect Off-QD assay to 550 nm emitting QDs capped with DHLA-PEG. Despite the potential for steric-size related self-assembly issues, QDs functionalized with these ligands are more amenable to assays using buffers that span a wide pH range while DHLA QDs are limited to only the basic pH range.[48,52] In these assays, the final ratios of peptide relative to QD were varied from 2.3 up to a valence of 8. Figure 5B shows the various resulting S/S_0 responses plotted as a function of the LcA concentration. The LODs determined from this data ranged from 0.14 to 0.69 nM LcA for the 2.3 and 8.0 ratios, respectively, with an overall average value of 0.35 ± 0.24 nM. These values are similar to the 0.08−1.4 nM LcA LODs determined in a previous study using a commercial FRET-based protease substrate in combination with a custom-built miniaturized fluorescent detection platform.[27]

Given the accumulating evidence for $(His)_6$-coordination to the surface of carboxylated ITK QDs,[25,36,40] we also tested whether these materials could assemble the LcA-pep-Cy3 and simultaneously allow direct-on QD digestion by LcA. Figure 5C shows S/N responses derived from 525 nm ITK QDs preassembled in Ni^{2+}-supplemented buffer with the indicated ratios of 5, 10, and 15 peptide substrates and exposed to increasing concentrations of LcA for 3 h. The increase in S/S_0 response from ≈ 1.5 to 3 for the different peptide ratios tested indicate that more peptide is productively available for enzyme interactions when assembled on these larger diameter nanoparticles. Figure 5D shows data collected and processed in the same manner for 545 nm ITK QDs self-assembled with the same ratios of LcA-pep-Cy3 and exposed to increasing concentrations of protease. Maximum S/S_0 ratios appear to plateau for all three ratios around 2.5. We note far larger error bars for this second data set which we partially ascribe to spectral overlap. The emissions of the QD donor and the Cy3 acceptor share significant spectral overlap (see Figures 2C and 4C) making deconvolution of the data more complicated and error prone. Clearly sensors assembled with ITK QDs facilitate direct On-QD assay formats, however, we found that the LODs determined from the dose response curves were less sensitive and ranged from 2.3 to 18.8 nM LcA for the 525 nm ITK QDs and 1.2−37.5 nM LcA for the 545 nm ITK QDs. The LOD was found to be dependent on ratio but not in any discernible pattern. For both the 525 and 545 nm ITK QDs 1:10 QD/LcA-pep-Cy3 was found to have the worst LOD of the three ratios tested. In terms of estimating actual turnover activity, converting the data shown in Figure 5 to units of maximum apparent enzymatic velocity ($V_{max.app.}$) derive values which fall in the range of 10−100 pM peptide cleaved per min depending upon ratio and format used.[21,23]

Modeling Quantum Dot−Peptide Structures. We have previously shown that modeling QD−protein/peptide systems provides insight into the assembly nanoarchitecture and the influence this can subsequently exert on function.[21,44,53,54] Models are compiled by considering the relevant information available on the QDs, how the peptides interact with the QDs and what has been previously determined about the peptide structure. Figure 6A shows the model derived for the LcA-pep-Cy3 as self-assembled onto the DHLA/DHLA-PEG functionalized QDs. The CdSe−ZnS core−shell structure is simulated by the central blue sphere of radius ~30 Å which corresponds to the size appropriate for 550 nm emitting QDs. The DHLA ligand shell is shown by the magenta sphere with an extension of 12 Å surrounding the QD. The DHLA-PEG ligand shell is also shown in gray and extends away 38 Å from the QD

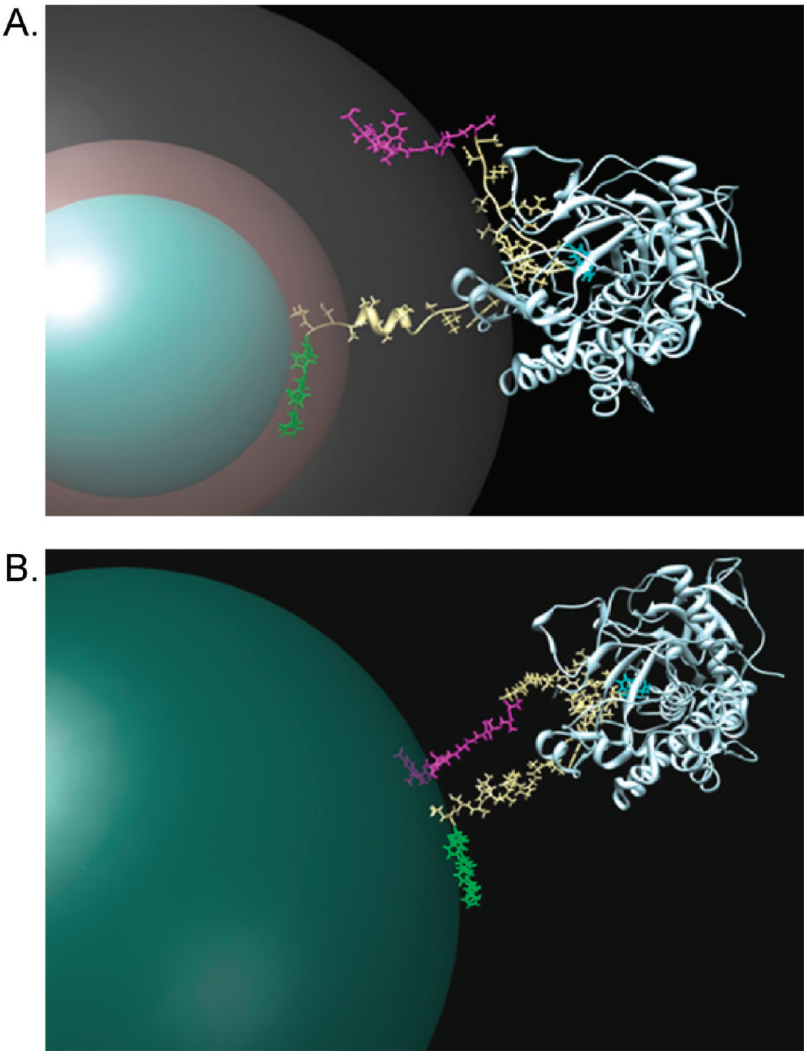

Figure 6. Models of QD−peptide structures. (A) Model of LcA-pep-Cy3 self-assembled onto DHLA/DHLA-PEG functionalized 550 nm emitting QDs. 550 nm emitting QD core−shell structure is simulated by the central blue sphere of ~30 Å radius. The DHLA ligand shell is shown as the magenta sphere extending 12 Å around the QD. The DHLA-PEG ligand shell is shown in gray and extends 38 Å from the QD surface. The peptides C-terminal $(His)_6$ shown in green is in direct contact with the ZnS shell. The helical spacer segment of the peptide is in yellow. The QRATKM portion of the peptide is constrained into a highly bent conformation as found in the native SNAP-25 protein. The QR residues cleaved by the LcA protease are shown in cyan. The N-terminal Cy3 fluorophore is shown in magenta with its center placed at ~56 Å from the QD center as estimated from FRET studies. This model highlights the strong probability that Cy3 will penetrate the DHLA-PEG shell in this position. The ~50 kD LcA protein structure is shown in a ribbon and helix structure superimposed over the peptide in white. (B) Model derived for LcA-pep-Cy3 self-assembled onto the commercial ITK QDs. A sphere with radius 75 Å simulates the QD core−shell polymer structure. The $(His)_6$ in green is attached to chelated Ni^{2+} coordinated by surface carboxyl groups. The Cy3 fluorophore is located with its center ~74 Å from the QD center as estimated from the FRET data showing the possibility of some interpenetration of the QD-polymer coating. The LcA protein is depicted superimposed over the peptide as a white ribbon and helix structure.

surface. The peptides C-terminal $(His)_6$ metal-affinity domain is shown in green in direct contact with the ZnS shell.[31] The helical spacer segment of the peptide in yellow is displayed laterally extending away from the QD surface. The QRATKM portion of the peptide is then constrained into the same highly bent conformation as found in the crystallographic structure of the SNAP-25 fragment bound by the LcA protein. The QR residues cleaved by the LcA protease are shown in cyan. The N-terminal Cy3 fluorophore is shown in magenta with its center placed at ~56 Å from the QD center. This distance was estimated from the FRET studies and is meant to highlight the fact that there is a high probability it will penetrate a portion of the DHLA-PEG shell at this position. The ~50 kD LcA protein structure is shown in a ribbon and helix structure superimposed over the peptide in white. The protein conformation was adjusted to match known interactions with the SNAP-25 fragment.

Figure 6B shows the same peptide as attached to an ITK QD. In this case, as very little is known about the proprietary QD coating, a sphere of 150 Å diameter (http://probes.invitrogen.com/media/pis/mp19000.pdf) is used to simulate the QD core−shell covered by the polymer. It is assumed that the $(His)_6$ portion of the

peptide does not penetrate far into the polymer coating and is attached to chelated Ni^{2+} coordinated by several (surface) carboxyl groups. This is reflected by its placement at the spheres periphery and is supported by data from several recent studies.[25,36,40] The terminal Cy3 fluorophore is located with its center placed at ~74 Å from the QD center as estimated from the FRET data; this may lead to some penetration of the polymer. The LcA protein is again depicted superimposed over the peptide as a white ribbon and helix structure matched to known interactions. Interestingly, besides altering the Cy3 into a longer, more linear conformation to match the FRET data, nothing else in the peptide sequence is altered structurally when attached to these nanoparticles as compared to the above simulation. It is important to note that in both models, the peptide has a wide freedom of rotation relative to the QD and these static models represent only one of several possible conformations. We do know the point of peptide attachment to the QD, or QD surface for the ITK materials, and the FRET data collected from each structure only reports where the acceptor dye is probably located. The location of the rest of the intervening peptide has to be qualified as more speculative.

In examining the models, several salient points can be drawn about the effects of architecture on overall sensor function. First, exact length and sequence of the SNAP-25 substrate used is critically important for recognition and cleavage by LcA. Testing with the minimal initial peptide substrate sequence confirmed that a slightly extended recognition sequence where the central glutamic acid had also been switched to glutamine is necessary for activity (see Figure 1B). Second, the recognition and cleavage sequence in the substrate should be presented to the LcA in the native "bent" conformation similar to that found in the SNAP-25/LcA interaction. Third, this critical sequence/structure must be sufficiently extended away, *via* a long helical linker in this case, from the QD surface and ligand coating to allow the LcA binding site access to the peptide without being hindered by interactions with the QD surface coating. Assays with the DHLA/DHLA-PEG QDs where exposure of preassembled QD−peptide sensors to ~50 kD LcA did not result in any proteolysis strongly suggest that the large LcA structure with its relatively deep active-site pocket is sterically precluded from productive interactions with the peptide substrate even when assembled to QDs displaying the smaller DHLA capping ligand. In contrast, exposing the same composite structures to 24 kD trypsin resulted in cleavage as did pre-exposing the peptide to LcA prior to QD assembly. Assay results also strongly support the idea that the LcA-pep-Cy3 is coordinated at or near the surface of the ITK QDs; had the peptide coordinated deep in the polymer coating the LcA would not have had unhindered binding access and would have been able to cleave to the substrate. A model of the initial peptide sequence coordinated to DHLA QDs and assembled using the same approach also suggests that lateral extension away from the QD is important (see Supporting Information, Figure 1). Lastly, the location of the acceptor fluorophore relative to the peptide is not critical as long as it does not hinder overall function by blocking self-assembly to the QDs or preventing LcA binding to the peptide substrate. Overall, assay results and modeling highlight how both peptide sequences and final sensor architecture can be critical to function and that iterative testing and redesign of substrates may be necessary.

CONCLUSIONS

Interest in utilizing QDs within active sensing platforms exploiting FRET or other sensing modalities continues to drive their evolution and the transition from *in vitro* to *in vivo* formats.[17] Myriad analytes and active processes have been successfully targeted with such assemblies including nutrients, explosives, drugs, proteins, peptides, nucleic acids, cofactors, second messenger ions, proteases, kinases, and pH.[17,55−57] As more types of QD materials become widely available, these opportunities will only expand. However, it is clear that concomitant with this will be a need for careful design and a full understanding of their structure−function relationship. As reported here, QD−peptide FRET-based proteolytic sensing can be extended to assemblies incorporating lengthy recognition/substrate sequences. Indeed, the currently utilized 16-residue SNAP-25 fragment is 4 times longer than the minimal DEVD sequence used to target caspase 3 previously.[22,30] We also find that differences in QD physiochemical properties, especially the nature of their surface ligands, have significant repercussions on sensor function. The ability of ITK-carboxyl QDs to self-assemble LcA-pep-Cy3 on or very near their surface presumably allows the LcA enzyme unfettered access to the substrate sequence while still providing for efficient FRET. This key property allows the assemblies to be directly incorporated as active sensors into the assay. In contrast, the nature of the DHLA ligands precludes this type of assay and results in these types of functionalized QDs being used in a slightly different role. Within the indirect Off-QD format, the QDs are essentially utilized as a development or visualization reagent which is added following proteolysis. Although requiring some extra steps, the benefit of this format is the *ca.* 10-fold gain in sensitivity. This difference also suggests that there may be subtle steric inhibition contributions still present in the QD−ITK sensor assembly.

Utilizing QDs as an integral part of FRET-based sensors targeting LcA, or other serotype-specific BoNTs, provides unique access to properties unavailable to conventional peptide substrates which typically display a single-donor/single-acceptor dye configuration. QD photophysical and chemical stability may also allow similar assays to be easily transitioned

into LOC devices for field deployment.[13,23] The LcA LOD of 0.35 nM (17.5 ng/mL) achieved in just this initial evaluation is comparable to many of the immuno- and activity-based assays described in the literature.[2,3] More importantly, all the sensors described here in their different formats were constructed using the most facile chemical-approach available, namely self-assembly.

MATERIALS AND METHODS

Materials. All chemicals were reagent grade and used as received from the manufacturer. *N*-(2-Hydroxyethyl)piperazine-*N*′-(2-ethanesulfonic acid) (HEPES), phosphate buffered saline (137 mM NaCl, 10 mM phosphate, 2.7 mM KCl, pH 7.4, PBS), imidazole, HPLC grade acetonitrile, Tween-20, and Corning 96-well white polystyrene nonbinding surface (NBS) plates were obtained from Sigma-Aldrich (St. Louis, MO). Nickel-nitrilotriacetic acid (Ni-NTA) agarose media was purchased from Qiagen (Valencia, CA). Oligonucleotide purification cartridges (OPC) and triethylamine acetate buffer (TEAA) were obtained from Applied Biosystems (Foster City, CA). Cy3-maleimide monoreactive dye was purchased from Amersham Biosciences (Piscataway, NJ). The active recombinant light chain of Botulinum Neurotoxin A (LcA, MW ≈ 49.98 kD) was obtained from List Biological Laboratories (Campbell, CA). Trypsin from bovine pancreas (MW ≈ 24 kDa, 10 000 BAEE units/mg) was obtained from Sigma-Aldrich. Doubly distilled water (ddH_2O) was obtained from a Nanopure Diamond water purification system (Barnstead, Dubuque, IA).

Semiconductor Quantum Dots. CdSe−ZnS core−shell QDs with emission maxima centered at 550 nm were synthesized using a stepwise reaction of organometallic precursors in hot coordinating solvent mixtures following the procedures described in refs 58 and 59. Nanocrystals were made hydrophilic by exchanging the native capping shell of trioctyl phosphine and trioctyl phosphine oxide (TOP/TOPO) with either dihydrolipoic acid (DHLA) or poly(ethylene glycol)-appended DHLA ligands terminating in a methoxyl group (DHLA-PEG-OMe, PEG MW ≅ 750) as described in ref 48 and 52 (see Figure 1 for chemical structures). CdSe−ZnS core−shell Qdot 525 and 545 Innovators Tool Kit (ITK) carboxylated QDs were purchased from Life Technologies (Eugene, OR). QD absorption and emission spectra are shown in Figure 2.

Peptide Synthesis and Labeling. The LcA peptide substrate sequences (LcA-pep) were synthesized using standard *in situ* neutralization cycles for Boc-solid-phase-peptide synthesis (Boc-SPPS) as described[60,61] and are shown in Figure 1. A discussion of peptide structure and function is provided in the Results and Discussion. Peptide labeling and purification procedures are described extensively in ref 23. Briefly, 1 mg peptide was dissolved in 1 mL of 10× PBS and combined with excess Cy3-maleimide monoreactive dye overnight at 4 °C. Unreacted Cy3 dye was removed by loading the reaction onto three consecutive 0.5 mL columns of Ni-NTA-agarose. Columns were washed with 10 mL of PBS before the labeled peptide was eluted with 300 mM imidazole in PBS. Cy3-labeled peptide (LcA-pep-Cy3) was desalted and imidazole was removed using a reverse-phase OPC. The cartridge was primed by washing first with 3 mL of acetonitrile followed by 3 mL of 2 M TEAA before loading LcA-pep-Cy3. The column was then washed with 50 mL of 0.02 M TEAA, and the LcA-pep-Cy3 was eluted, using 1 mL of 70% acetonitrile in ddH_2O. If needed, further rounds of sample purification were performed after the OPC was regenerated by washing again with 3 mL of acetonitrile followed by 3 mL of 2 M TEAA. The desalted Cy3-LcA-pep was characterized by UV−visible spectroscopy (Cy3 absorbance 150 000 M^{-1} cm^{-1} at 550 nm) before being aliquoted, dried down, and stored in a desiccator at −20 °C until required.

Quantum Dot−Peptide FRET and LcA Proteolytic Assays. Fluorescent data from FRET titrations and enzyme assays were collected using either a Tecan Safire or a Tecan Infinite M1000 Dual Monochromator Multifunction Plate Reader (Tecan, Research Triangle Park, NC) from samples aliquoted into 96 well microtiter plates. Different QD preparations with different emissions were investigated during this study including 550 nm emitting QDs solubilized with either DHLA or DHLA-PEG, as described above, along with commercial 525 and 545 ITK carboxyl QDs. FRET interactions between the various QDs and the Cy3-acceptor labeled peptide were first evaluated by self-assembling an increasing molar ratio of dye-labeled peptide per QD sample. LcA-pep-Cy3 was resuspended by dissolving in DMSO (∼5% of the final volume) followed by ddH_2O such that the final concentration was 100 μM. Between 15 and 30 pmoles of the 550 nm emitting DHLA/DHLA-PEG QD samples were mixed with LcA-pep-Cy3 at molar ratios of peptide-to-QD ranging from 0 to 10 in 20 mM HEPES + 0.1% Tween-20 pH 8.0 (HEPES buffer). Alternatively, 1.75 pmoles of the ITK carboxyl QDs were mixed with LcA-pep-Cy3 at molar ratios of peptide-to-QD ranging from 0 to 30 in the same HEPES buffer supplemented with 0.25 mM $NiCl_2$. Control experiments demonstrated minimal to no Ni^{2+} quenching of the QDs at this concentration (data not shown) similar to previous testing with the same ITK carboxyl QDs (Supporting Figure 5 in ref 36). Solutions were incubated at room temperature (RT) for 30 min before analysis. Control samples consisting of equivalent amounts of free Cy3 dye alone and QDs with free Cy3 were also monitored to account for the direct excitation component to the acceptor dye and to investigate solution-based FRET interactions.

For the LcA enzymatic assays, two formats were utilized as summarized in the assay scheme depicted in Figure 1A. In the On-QD (1-step) assay, QDs were first assembled with a fixed ratio of LcA-pep-Cy3 in HEPES buffer (and Ni^{2+} for ITK QDs) for ∼30 min at RT. The QD:LcA-pep-Cy3 constructs were mixed with the indicated concentrations of LcA enzyme, or no enzyme control, and loaded into 96-well plates for fluorescent measurement after incubation at 37 °C for 2 to 3 h. No significant differences in results were observed when using either 2 or 3 h. For the Off-QD (two-step) assay, the LcA-pep-Cy3 is first incubated with the indicated concentrations of LcA enzyme, or no enzyme control, for the same 2−3 h at 37 °C, and then the appropriate QD solution is added such that a specific QD:LcA-pep-Cy3 ratio is obtained in the final solution. Here, the QD−peptide samples are allowed to incubate for ∼30 min before being loaded into a 96-well plate for fluorescent measurement. All assay points were performed in duplicate to triplicate and standard deviations are shown where appropriate.

Data Analysis. Experimentally, FRET efficiency E_n (where n is the ratio or valence of dye-acceptors per QD) was determined using

$$E_n = \frac{(F_D - F_{DA})}{F_D} \quad (1)$$

where F_D and F_{DA} designate the integrated fluorescence intensities of donor alone and donor in the presence of acceptor(s), respectively.[62] Note: peak heights may also be used and yield similar values. Data from FRET efficiency were then analyzed within the Förster formalism to determine values for center-to-center (QD-to-dye) separation distance r using eq 2 which assumes a centro-symmetric distribution of dye-acceptors around a central QD:[16,18]

$$r = \left(\frac{n(1-E_n)}{E}\right)^{1/6} R_0 \quad (2)$$

R_0 designates the Förster distance corresponding to a FRET efficiency E of 50% for a single QD-donor donor/single dye-acceptor ratio.[62] Because of the occurrence of high FRET efficiencies measured for sample sets at relatively low ratios, heterogeneity in conjugate self-assembly valence was also accounted for where applicable. We use a Poisson distribution function, $p(k,n)$, to describe the heterogeneity in conjugate

valence where FRET E in eq 2 is further written as[41]

$$E(n) = \sum_{k=1}^{n} p(k, n)\, E(k) \quad \text{with} \quad p(k, n) = \frac{e^{-n} n^k}{k!} \qquad (3)$$

where n is the average acceptor-to-QD ratio used during reagent mixing and k is the exact number of peptide-dye conjugated to the QD. This allows us to estimate any deviation in the observed FRET E and was only applied for ratios of $n \leq 5$ where this issue is expected to manifest. For analyses of enzymatic data, changes in FRET E were converted to a signal-overbackground or S/S_0 ratio response by dividing the QD donor PL from the enzyme exposed QD:LcA-pep-Cy3 construct (S) by the QD donor PL of the zero enzyme control (*i.e.*, QD:LcA-pep-Cy3 construct not exposed to LcA-S_0).

Structural Modeling. Hybrid QD−peptide models were created with UCSF Chimera version 1.4.1 using a process similar to that previously described.[21,44,53,54] Energy minimization was also carried out in Chimera using ANTECHAMBER (Version 1.27) and the AM1-BCC method of calculating charges. The LcA crystallographic structure selected was Protein Data Bank (www.rcsb.org/pdb) entry 3DDA which has a fragment of the SNAP25 protein substrate cocrystallized in the binding site. This entry was also used to identify the critical residues important for LcA−peptide substrate interactions. The SNAP25 fragment conformation was further used as a guide to adjust torsion angles in the Gln-Arg-Ala-Thr-Lys(-Met) subsequence of the peptide substrate(s) into the appropriate "bent" conformation. Peptide structures were then docked to the surface of the QD *via* the terminal $(His)_6$ metal-affinity sequence. The conformation of the peptide on the QD was then adjusted by moving the helical spacer portion to reflect QD donor/Cy3 acceptor center-to-center distances in agreement with those experimentally determined from FRET data. Lastly, the LcA 3-D structure was superimposed over the bent peptide with its binding site matched to the appropriate substrate residues and final images were rendered in Adobe Photoshop.

Acknowledgment. The authors acknowledge the NRL-NSI, ONR, DTRA and the Office of Public Health Emergency Preparedness and FDA contract HHSF223200610765P for financial support. Molecular graphics images were produced using the UCSF Chimera package from the Resource for Biocomputing, Visualization, and Informatics at the University of California, San Francisco (supported by NIH P41 RR-01081). J.B.B.-C. acknowledges a Marie Curie IOF.

Supporting Information Available: A model of the Cy3-labeled initial peptide sequence as self-assembled to 550 nm emitting DHLA-functionalized QDs. This material is available free of charge *via* the Internet at http://pubs.acs.org.

REFERENCES AND NOTES

1. Brunger, A. T.; Rummel, A. Receptor and Substrate Interactions of Clostridial Neurotoxins. *Toxicon* **2009,** *54*, 550–560.
2. Wictome, M.; Shone, C. C. Botulinum Neurotoxins: Mode of Action and Detection. *J. Appl. Microbiol. Symp. Suppl.* **1998,** *84*, 87S–97S.
3. Cai, S.; Singh, B. R.; Sharma, S. Botulism Diagnosis: From Clinical Symptoms to *in Vitro* Assays. *Clin. Rev. Microbiol.* **2007,** *33*, 109–125.
4. Fu, Z.; Chen, S.; Bladwin, M. R.; Boldt, G. E.; Crawford, A.; Janda, K. D.; Barbieri, J. T.; Kim, J.-J. P. Light Chain of Botulinum Neurotixin Serotype a: Structural Resolution of a Catalytic Intermediate. *Biochem.* **2006,** *45*, 8903–8911.
5. Hicks, R. P.; Hartell, M. G.; Nichols, D. A.; Bhattacharjee, A. K.; van Hamont, J. E.; Skillman, D. R. The Medicinal Chemistry of Botulinum, Ricin and Anthrax Toxins. *Cur. Med. Chem.* **2005,** *12*, 667–690.
6. Hakami, R. M.; Ruthel, G.; A.M., S.; Bavari, S. Gaining Ground: Assays and Therapeutics against Botulinum Neurotoxin. *Trends Microbiol.* **2010,** *18*, 164–172.
7. Swain, M. D.; Anderson, G. P.; Zabetakis, D.; Bernstein, R. D.; Liu, J. L.; Sherwood, L. J.; Hayhurst, A.; Goldman, E. R. Llama-Derived Single-Domain Antibodies for the Detection of Botulinum a Neurotoxin. *Anal. Bioanal. Chem.* **2010,** *398*, 339–348.
8. Kalb, S. R.; Smith, T. J.; Moura, H.; Hill, K.; Lou, J. L.; Geren, I. N.; Garcia-Rodriguez, C.; Marks, J. D.; Smith, L. A.; Pirkle, J. L.; Barr, J. R. The Use of Endopep-MS to Detect Multiple Subtypes of Botulinum Neurotoxins A, B, E, and F. *Int. J. Mass Spectrom.* **2008,** *278*, 101–108.
9. Marconi, S.; Ferracci, G.; Berthomieu, M.; Kozaki, S.; Miquelis, R.; Boucraut, J.; Michael, S. B.; Leveque, C. A Protein Chip Membrane-Capture Assay for Botulinum Neurotoxin Activity. *Toxicol. Appl. Pharmacol.* **2008,** *233*, 439–446.
10. Schmidt, J. J.; Stafford, R. G. Fluorigenic Substrates for the Protease Activities of Botulinum Neurotoxins, Serotypes A, B, and F. *Appl. Environ. Microbiol.* **2003,** *69*, 297–303.
11. Bagramyan, K.; Barash, J. R.; Arnon, S. S.; Kalkum, M. Attomolar Detection of Botulinum Toxin Type A in Complex Biological Matrices. *PLoS ONE* **2008,** *3*, e2041.
12. Mangru, S.; Bentz, B. L.; Davis, T. J.; Desai, N.; Stabile, P. J.; Schmidt, J. J.; Millard, C. B.; Bavari, S.; Kodukula, K. Integrated Bioassays in Microfluidic Devices: Botulinum Toxin Assays. *J. Biomol. Screening* **2005,** *10*, 788–794.
13. Sun, S.; Ossandon, M.; Kostov, Y.; Rasooly, A. Lab-on-a-Chip for Botulinum Neurotoxin A (BoNT-A) activity analysis. *Lab Chip* **2009,** *9*, 3275–3281.
14. Kupstat, A.; Kumke, M. U.; Hildebrandt, N. Toward Sensitive, Quantitative Point-of-Care (POCT) of Protein Markers: Miniaturization of a Homogeneous Time-Resolved Fluoroimmunoassay for Prostate-Specific Antigen Detection. *Analyst* **2011**, *136*, 1029−1035.
15. Sapsford, K. E.; Berti, L.; Medintz, I. L. Materials for Fluorescence Resonance Energy Transfer: Beyond Traditional "Dye to Dye" Combinations. *Angew. Chem., Int. Ed.* **2006,** *45*, 4562–4588.
16. Medintz, I. L.; Mattoussi, H. Quantum Dot-Based Resonance Energy Transfer and Its Growing Application in Biology. *Phys. Chem. Chem. Phys.* **2009,** *11*, 17–45.
17. Algar, W. R.; Krull, U. J. New Opportunities in Multiplexed Optical Bioanalyses Using Quantum Dots and Donor-Acceptor Interactions. *Anal. Bioanal. Chem.* **2010,** *398*, 2439–2449.
18. Clapp, A. R.; Medintz, I. L.; Mauro, J. M.; Fisher, B. R.; Bawendi, M. G.; Mattoussi, H. Fluorescence Resonance Energy Transfer between Quantum Dot Donors and Dye-Labeled Protein Acceptors. *J. Am. Chem. Soc.* **2004,** *126*, 301–310.
19. Geissler, D.; Charbonnière, L. J.; Ziessel, R. F.; Butlin, N. G.; Löhmannsröben, H.-G.; Hildebrandt, N. Quantum Dot Biosensors for Ultrasensitive Multiplexed Diagnosis. *Angew. Chem., Int. Ed.* **2010,** *49*, 1396–1401.
20. Morgner, F.; Geissler, D.; Stufler, S.; Butlin, N. G.; Löhmannsröben, H.-G.; Hildebrandt, N. A Quantum-Dot-Based Molecular Ruler for Multiplexed Optical Analysis. *Angew. Chem., Int. Ed.* **2010,** *49*, 7570–7574.
21. Medintz, I. L.; Clapp, A. R.; Brunel, F. M.; Tiefenbrunn, T.; Uyeda, H. T.; Chang, E. L.; Deschamps, J. R.; Dawson, P. E.; Mattoussi, H. Proteolytic Activity Monitored by Fluorescence Resonance Energy Transfer through Quantum-Dot-Peptide Conjugates. *Nat. Mater.* **2006,** *5*, 581–589.
22. Boeneman, K.; Mei, B.; Dennis, A.; Bao, G.; Deschamps, J. R.; Mattoussi, H.; Medintz, I. L. Sensing Caspase 3 Activity with Quantum Dot-Fluorescent Protein Assemblies. *J. Am. Chem. Soc.* **2009,** *131*, 3828–3829.
23. Sapsford, K. E.; Farrell, D.; Sun, S.; Rasooly, A.; Mattoussi, H.; Medintz, I. L. Monitoring of Enzymatic Proteolysis on a Electroluminescent-CCD Microchip Platform Using Quantum Dot−Peptide Substrates. *Sens. Actuators, B* **2009,** *139*, 13–21.
24. Shi, L.; Rosenzweig, N.; Rosenzweig, Z. Luminescent Quantum Dots Fluorescence Resonance Energy Transfer-Based Probes for Enzymatic Activity and Enzyme Inhibitors. *Anal. Chem.* **2007,** *79*, 208–214.
25. Yao, H.; Zhang, Y.; Xiao, F.; Xia, Z.; Rao, J. Quantum Dot/Bioluminescence Resonance Energy Transfer Based Highly Sensitive Detection of Proteases. *Angew. Chem., Int. Ed.* **2007,** *46*, 4346–4349.
26. Schmidt, J. J.; Bostian, K. A. Endoproteinase Activity of Type A Botulinum Neurotoxin: Substrate Requirements and Activation by Serum Albumin. *J. Protein Chem.* **1997,** *16*, 19–26.
27. Sun, S.; Francis, J.; Sapsford, K. E.; Kostov, Y.; Rasooly, A. Multi-Wavelength Spatial LED Illumination Based Detector

for *in Vitro* Detection of Botulinum Neurotoxin A Activity. *Sens. Actuators, B* **2010,** *146*, 297–306.
28. Shi, Z. S.; Olson, C. A.; Bell, A. J.; Kallenbach, N. R. Stabilization of α-Helix Structure by Polar Side-Chain Interactions: Complex Salt Bridges, Cation−π Interactions, and C-H···O H-bonds. *Biopolymers* **2001,** *60*, 366–380.
29. Prasuhn, D. E.; Blanco-Canosa, J. B.; Vora, G. J.; Delehanty, J. B.; Susumu, K.; Mei, B. C.; Dawson, P. E.; Medintz, I. L. Combining Chemoselective Ligation with Polyhistidine-Driven Self-Assembly for the Modular Display of Biomolecules on Quantum Dots. *ACS Nano* **2010,** *4*, 267–278.
30. Prasuhn, D. E.; Feltz, A.; Blanco-Canosa, J. B.; Susumu, K.; Stewart, M. H.; Mei, B. C.; Yakovlev, A. V.; Loukov, C.; Mallet, J. M.; Oheim, M.; Dawson, P. E.; Medintz, I. L. Quantum Dot Peptide Biosensors for Monitoring Caspase 3 Proteolysis and Calcium Ions. *ACS Nano* **2010,** *4*, 5487–5497.
31. Sapsford, K. E.; Pons, T.; Medintz, I. L.; Higashiya, S.; Brunel, F. M.; Dawson, P. E.; Mattoussi, H. Kinetics of Metal-Affinity Driven Self-Assembly between Proteins or Peptides and CdSe-ZnS Quantum Dots. *J. Phys. Chem. C* **2007,** *111*, 11528–11538.
32. Dennis, A. M.; Bao, G. Quantum Dot-Fluorescent Protein Pairs as Novel Fluorescence Resonance Energy Transfer Probes. *Nano Lett.* **2008,** *8*, 1439–1445.
33. Dif, A.; Henry, E.; Artzner, F.; Baudy-Floc'h, M.; Schmutz, M.; Dahan, M.; Marchi-Artzner, V. Interaction between Water-Soluble Peptidic CdSe/ZnS Nanocrystals and Membranes: Formation of Hybrid Vesicles and Condensed Lamellar Phases. *J. Am. Chem. Soc.* **2008,** *130*, 8289–8296.
34. Liu, W.; Howarth, M.; Greytak, A. B.; Zheng, Y.; Nocera, D. G.; Ting, A. Y.; Bawendi, M. G. Compact Biocompatible Quantum Dots Functionalized for Cellular Imaging. *J. Am. Chem. Soc.* **2008,** *130*, 1274–84.
35. Berti, L.; D'Agostino, P. S.; Boeneman, K.; Medintz, I. L. Improved Peptidyl Linkers for Self-Assembling Semiconductor Quantum Dot Bioconjugates. *Nano Res.* **2009,** *2*, 121–129.
36. Boeneman, K.; Delehanty, J. B.; Susumu, K.; Stewart, M. H.; Medintz, I. L. Intracellular Bioconjugation of Targeted Proteins with Semiconductor Quantum Dots. *J. Am. Chem. Soc.* **2010,** *132*, 5975–5977.
37. Yeh, H. Y.; Yates, M. V.; Mulchandania, A.; Chen, W. Molecular Beacon-Quantum Dot−Au Nanoparticle Hybrid Nanoprobes for Visualizing Virus Replication in Living Cells. *Chem. Commun.* **2010,** *46*, 3914–3916.
38. Wu, X.; Liu, H.; Liu, J.; Haley, K. N.; Treadway, J. A.; Larson, J. P.; Ge, N.; Peale, F.; Bruchez, M. P. Immunofluorescent Labeling of Cancer Marker Her2 and Other Cellular Targets with Semiconductor Quantum Dots. *Nat. Biotechnol.* **2003,** *21*, 41–46.
39. Ueda, E. K. M.; Gout, P. W.; Morganti, L. Current and Prospective Applications of Metal Ion−Protein Binding. *J. Chromatogr. A* **2003,** *988*, 1–23.
40. Dennis, A. M.; Sotto, D.; Mei, B. C.; Medintz, I. L.; Mattoussi, H.; Bao, G. Surface Ligand Effects on Metal-Affinity Coordination to Quantum Dots: Implications for Nanoprobe Self-Assembly. *Bioconjugate Chem.* **2010,** *21*, 1160–1170.
41. Pons, T.; Medintz, I. L.; Wang, X.; English, D. S.; Mattoussi, H. Solution-Phase Single Quantum Dot Fluorescence Resonant Energy Transfer Sensing. *J. Am. Chem. Soc.* **2006,** *128*, 15324–15331.
42. Pons, T.; Uyeda, H. T.; Medintz, I. L.; Mattoussi, H. Hydrodynamic Dimensions, Electrophoretic Mobility and Stability of Hydrophilic Quantum Dots. *J. Phys. Chem. B* **2006,** *110*, 20308–20316.
43. Prasuhn, D. E.; Deschamps, J. R.; Susumu, K.; Stewart, M. A.; Boeneman, K.; Blanco-Canosa, J. B.; Dawson, P. E.; Medintz, I. L. Polyvalent Display and Packing of Peptides and Proteins on Semiconductor Quantum Dots: Predicted *versus* Experimental Results. *Small* **2009,** *6*, 555–564.
44. Medintz, I. L.; Pons, T.; Susumu, K.; Boeneman, K.; Dennis, A.; Farrell, D.; Deschamps, J. R.; Melinger, J. S.; Bao, G.; Mattoussi, H. Resonance Energy Transfer between Luminescent Quantum Dots and Diverse Fluorescent Protein Acceptors. *J. Phys. Chem. C* **2009,** *131*, 18552–18561.
45. Mattoussi, H.; Mauro, J. M.; Goldman, E. R.; Anderson, G. P.; Sundar, V. C.; Mikulec, F. V.; Bawendi, M. G. Self-Assembly of CdSe−ZnS Quantum Dot Bioconjugates Using an Engineered Recombinant Protein. *J. Am. Chem. Soc.* **2000,** *122*, 12142–12150.
46. Abad, J. M.; Mertens, S. F. L.; Pita, M.; Fernandez, V. M.; Schiffrin, D. J. Functionalization of Thioctic Acid-Capped Gold Nanoparticles for Specific Immobilization of Histidine-Tagged Proteins. *J. Am. Chem. Soc.* **2005,** *127*, 5689–5694.
47. Uyeda, H. T.; Medintz, I. L.; Jaiswal, J. K.; Simon, S. M.; Mattoussi, H. Synthesis of Compact Multidentate Ligands to Prepare Stable Hydrophilic Quantum Dot Fluorophores. *J. Am. Chem. Soc.* **2005,** *127*, 3870–3878.
48. Mei, B. C.; Susumu, K.; Medintz, I. L.; Mattoussi, H. Polyethylene Glycol-Based Bidentate Ligands To Enhance Quantum Dot and Gold Nanoparticle Stability in Biological Media. *Nat. Protocols* **2009,** *4*, 412–423.
49. Susumu, K.; Uyeda, H. T.; Medintz, I. L.; Pons, T.; Delehanty, J. B.; Mattoussi, H. Enhancing the Stability and Biological Functionalities of Quantum Dots *via* Compact Multifunctional Ligands. *J. Am. Chem. Soc.* **2007,** *129*, 13987–13996.
50. Medintz, I. L.; Berti, L.; Pons, T.; Grimes, A. F.; English, D. S.; Alessandrini, A.; Facci, P.; Mattoussi, H. A Reactive Peptidic Linker for Self-Assembling Hybrid Quantum Dot−DNA Bioconjugates. *Nano Lett.* **2007,** *7*, 1741–1748.
51. Zhang, C. Y.; Johnson, L. W. Quantum Dot-Based Fluorescence Resonance Energy Transfer with Improved FRET Efficiency in Capillary Flows. *Anal. Chem.* **2006,** *78*, 5532–5537.
52. Mei, B. C.; Susumu, K.; Medintz, I. L.; Delehanty, J. B.; Mountziaris, T. J.; Mattoussi, H. Modular Poly(Ethylene Glycol) Ligands for Biocompatible Semiconductor and Gold Nanocrystals with Extended pH and Ionic Stability. *J. Mater. Chem.* **2008,** *18*, 4949–4958.
53. Medintz, I. L.; Konnert, J. H.; Clapp, A. R.; Stanish, I.; Twigg, M. E.; Mattoussi, H.; Mauro, J. M.; Deschamps, J. R. A Fluorescence Resonance Energy Transfer Derived Structure of a Quantum Dot−Protein Bioconjugate Nanoassembly. *Proc. Natl. Acad. Sci. U.S.A.* **2004,** *101*, 9612–9617.
54. Goldman, E.; Medintz, I.; Whitley, J.; Hayhurst, A.; Clapp, A.; Uyeda, H.; Deschamps, J.; Lassman, M.; Mattoussi, H. A Hybrid Quantum Dot−Antibody Fragment Fluorescence Resonance Energy Transfer-Based TNT Sensor. *J. Am. Chem. Soc.* **2005,** *127*, 6744–6751.
55. Ghadiali, J. E.; Cohen, B. E.; Stevens, M. M. Protein Kinase-Actuated Resonance Energy Transfer in Quantum Dot−Peptide Conjugates. *ACS Nano* **2010,** *4*, 4915–4919.
56. Gill, R.; Zayats, M.; Willner, I. Semiconductor Quantum Dots for Bioanalysis. *Angew. Chem., Int. Ed.* **2008,** *47*, 7602–7625.
57. Algar, W. R.; Krull, U. J. Towards Multicolour Strategies for the Detection of Oligonucleotide Hybridization Using Quantum Dots as Energy Donors in Fluorescence Resonance Energy Transfer (FRET). *Anal. Chim. Acta* **2007,** *581*, 193–201.
58. Dabbousi, B. O.; Rodriguez-Viejo, J.; Mikulec, F. V.; Heine, J. R.; Mattoussi, H.; Ober, R.; Jensen, K. F.; Bawendi, M. G. (CdSe)ZnS Core−Shell Quantum Dots: Synthesis and Optical and Structural Characterization of a Size Series of Highly Luminescent Materials. *J. Phys. Chem. B* **1997,** *101*, 9463–9475.
59. Peng, Z. A.; Peng, X. Formation of High-Quality CdTe, CdSe, and CdS Nanocrystals Using CdO as Precursor. *J. Am. Chem. Soc.* **2001,** *123*, 183–184.
60. Schnolzer, M.; Alewood, P.; Jones, A.; Alewood, D.; Kent, S. B. *In Situ* Neutralization in Boc-Chemistry Solid Phase Peptide Synthesis. Rapid, High Yield Assembly of Difficult Sequences. *Int. J. Pept. Protein. Res.* **1992,** *40*, 180–193.
61. Delehanty, J. B.; Medintz, I. L.; Pons, T.; Brunel, F. M.; Dawson, P. E.; Mattoussi, H. Self-Assembled Quantum Dot−Peptide Bioconjugates for Selective Intracellular Delivery. *Bioconjugate Chem.* **2006,** *17*, 920–927.
62. Lakowicz, J. R. *Principles of Fluorescence Spectroscopy*, 3rd ed.; Springer: New York, 2006.